

ONR-URI Composites Program  
Technical Report No. 90-07

UIUC-NCCMR-90-07

2

**AD-A233 986**

**EFFECT OF A VISCOELASTIC INTERFACE ON  
THE TRANSVERSE BEHAVIOR OF  
FIBER-REINFORCED COMPOSITES**

M. Gosz, B. Moran and J. D. Achenbach

April, 1990

National Center for Composite Materials Research  
at University of Illinois, Urbana - Champaign  
A DoD University Research Initiatives Center funded by the  
Office of Naval Research, Arlington, VA

91 3 27 070

# EFFECT OF A VISCOELASTIC INTERFACE ON THE TRANSVERSE BEHAVIOR OF FIBER-REINFORCED COMPOSITES

M. GOSZ, B. MORAN and J. D. ACHENBACH  
Center for Quality Engineering and Failure Prevention  
Northwestern University  
Evanston, IL 60208-3020

**Abstract** – In this paper we investigate the effect of an inelastic interface layer on the mechanical behavior of a transversely loaded fiber-reinforced composite. A simple linearly viscoelastic model is used to characterize the stiffness and viscosity of the interface separating the fiber and matrix phases. The mechanical response is obtained using the finite element method and calculations are carried out for a unit cell in a periodic array of hexagonally packed fibers. An approximate representation of the time dependent macroscopic behavior of the composite is derived analytically and compared with the numerical results. From a micromechanical perspective, the influence of interfacial stress relaxation on the stress fields in the matrix material contiguous to the interface is examined.

## 1. INTRODUCTION

Since the advent of the modern fiber-reinforced composite, the determination of the mechanical properties of these materials has become of significant practical importance. Unlike the axial strength and stiffness properties which are primarily governed by the axial properties of the fiber, the behavior of the fiber-reinforced composite in the transverse direction is dominated by a relatively low stiffness matrix material and the fiber/matrix interface. This may place severe limitations on the overall performance of the composite and thus it is desirable to accurately characterize the transverse properties.

In most analytical and numerical work, investigators have assumed a perfect bond between the fibers and the matrix material which is modeled by continuity of interfacial tractions and displacements. In reality, however, a more complex state exists between the fiber and matrix constituents, and the assumption of perfect bonding may not be suitable in the presence of a thin interfacial zone which connects the two phases (e.g. fiber coating or intermolecular bonding). In this analysis it is assumed that the interface layer is infinitesimally thin and supports a traction field having both normal and tangential components. Continuity of tractions is assumed across the interface, however, fiber and matrix phase separation is simulated by allowing for displacement discontinuities across the interface. Such a model, assuming a linear relationship between the displacement difference across the interface and the conjugate tractions, is employed by Aboudi (1987),

DIST A PER TELECON MR. Y BARSOUM  
ONR/CODE 1132 SM  
4/1/91 CG

A-1



Steif and Hoysan (1987), Achenbach and Zhu (1989a,89b) and Hashin (1989). Needleman (1987) utilizes this model to simulate the bond between rigid spherical inclusions embedded in an isotropically hardening elastic-viscoplastic matrix and considers a more general interfacial constitutive relation.

In implementing the above mentioned interface model, care must be taken in order to avoid an unrealistic interpenetration of the matrix and fiber phases which can occur in local regions of compression. As will be seen later, the imposition of such a constraint significantly influences the transverse mechanical behavior of the composite with a relatively low stiffness interfacial zone.

In the present paper, the role of an inelastic interface on the transverse properties of the fiber-reinforced composite is considered from both a macroscopic and a microscopic perspective. The choice of a relatively simple linearly viscoelastic interface model allows us to derive an approximate representation for the transverse relaxation moduli of the composite with which to compare our numerical results. We note that this analytical model does not incorporate the aforementioned impenetrability constraint, and of primary interest is how well it compares with the numerical results over a range of interfacial stiffness parameters. In addition, the influence of interfacial stress relaxation on the stress fields in the matrix material contiguous to the interface is examined from a micromechanical viewpoint.

In the following section, the model which is chosen to represent the behavior of a unidirectional, fiber-reinforced composite is described and the boundary value problem is formulated. Discussed in section 3 are implementational details of the finite element method, the numerical procedure employed in this analysis. In section 4, the analytic model which approximates the transverse relaxation moduli of the fiber-reinforced composite is described and compared with the numerical results. In section 5, a qualitative discussion is presented regarding the effect of interfacial stress relaxation on the resulting stress fields in the matrix material near the fiber/matrix interface. Finally, some concluding remarks are stated in section 6.

## 2. FORMULATION OF THE BOUNDARY VALUE PROBLEM

A cross-sectional view of the model employed in this analysis is illustrated in figure 1. It is assumed that the fibers, all of equal radius,  $a$ , are periodically spaced in a regular hexagonal array and are embedded in an infinite matrix. Two loading directions are

considered in this analysis, the closest packing direction (CPD) and the mid-closest packing direction (Mid-CPD). The Mid-CPD loading direction which bisects the angle formed by two closest packing directions is illustrated in figure 1.

Through arguments of symmetry, it is only necessary to analyze the rectangular region outlined in figure 1 and shown in detail in figure 2. Neglecting all rigid body motion, the point  $O$ , located at the origin of the Cartesian coordinate system shown in the figure, is considered fixed throughout the analysis. By imposing the appropriate boundary conditions on one half of this rectangular region, i.e. the trapezoid  $ABEF$  consisting of one quarter of a regular hexagon with sides of length  $b$ , the state of stress and strain for the entire model may be completely characterized.

### 2.1. Boundary Conditions

The relevant boundary conditions for the case of CPD loading are given below. The corresponding expressions for the case of Mid-CPD loading are obtained similarly, see e.g. Achenbach and Zhu (1989b). Referring again to figure 2, the loading direction is parallel to the  $x_2$  axis of the Cartesian reference frame centered at  $O$ . Relative to this frame, the boundary conditions along the external boundaries  $AB$ ,  $EF$ , and  $AF$  respectively are expressed as follows:

$$x_1 \in \left[-\frac{3b}{4}, \frac{b}{4}\right], \quad x_2 = -\frac{\sqrt{3}}{4}b, \quad \sigma_{21} = 0, \quad u_2 = -\Delta_2 \quad (1)$$

$$x_1 \in \left[-\frac{3b}{4}, -\frac{b}{4}\right], \quad x_2 = +\frac{\sqrt{3}}{4}b, \quad \sigma_{21} = 0, \quad u_2 = +\Delta_2 \quad (2)$$

$$x_2 \in \left[-\frac{\sqrt{3}}{4}b, +\frac{\sqrt{3}}{4}b\right], \quad x_1 = -\frac{3b}{4}, \quad \sigma_{21} = 0, \quad u_1 = -\Delta_1 \quad (3)$$

where  $u_1$  and  $u_2$  are the displacement components in the  $x_1$  and  $x_2$  directions and  $\Delta_2$  is the magnitude of the prescribed displacement in the  $x_2$  direction along  $AB$  and  $EF$ . The quantity  $\Delta_1$  is the magnitude of the unknown displacement in the  $x_1$  direction along  $AF$  to be determined as part of the numerical solution. Along  $BE$ , the following displacement condition must hold:

$$u_1(-x_1, -x_2) = u_1(x_1, x_2), \quad u_2(-x_1, -x_2) = u_2(x_1, x_2). \quad (4)$$

One additional relevant condition for this case of loading is obtained through equilibrium considerations in the  $x_2$  direction and is stated as

$$\int_{AB} T_2 ds + \int_{EF} T_2 ds = \frac{3b}{2} \sigma_\infty \quad (5)$$

where  $T_2$  is the traction component in the  $x_2$  direction on the external boundaries  $AB$  and  $EF$ . This condition allows for the numerical determination of the remote applied stress  $\sigma_\infty$ .

## 2.2. Constitutive Relations

Now that the relevant conditions that must be satisfied on the external boundaries of the trapezoidal region  $ABEF$  have been given, we turn our attention to the individual material phases comprising the interior of the trapezoidal region. In the present analysis, a graphite/epoxy composite material system is considered, and a description of the constitutive law which governs the behavior of each phase follows.

*Epoxy Matrix and Graphite Fiber Phases.* It is assumed that the matrix is isotropic and linearly elastic. The fiber is taken to be linearly elastic and transversely isotropic. The elastic constants employed in this analysis were obtained by Kriz and Stinchcomb (1979) and are given in table 1. For the case of plane strain, the stress-strain relations for the matrix phase can be written as

$$\epsilon_{33} = \epsilon_{13} = \epsilon_{23} = 0 \quad (6)$$

$$\sigma_{13} = \sigma_{23} = 0$$

$$\sigma_{33} = \lambda(\epsilon_{11} + \epsilon_{22})$$

$$\sigma_{\alpha\beta} = 2\mu\epsilon_{\alpha\beta} + \lambda\epsilon_{\gamma\gamma}\delta_{\alpha\beta}$$

where the parameters  $\lambda$  and  $\mu$  are the Lamé' constants and the Greek indices  $\alpha$ ,  $\beta$ , and  $\gamma$  range over 1 and 2. For the transversely isotropic fiber phase, the elastic stress-strain relations for the case of plane strain are given by Hashin (1979). The non-zero components are written as

$$\sigma_{33} = l(\epsilon_{11} + \epsilon_{22}) \quad (7)$$

$$\sigma_{\alpha\beta} = (K_T - G_T)\epsilon_{\gamma\gamma}\delta_{\alpha\beta} + 2G_T\epsilon_{\alpha\beta}$$

where the constant  $l$  is related to the axial Poisson's ratio,  $\nu_A$ , and the transverse bulk modulus,  $K_T$ , by

$$l = 2K_T v_A \quad (8)$$

In addition, the transverse bulk modulus,  $K_T$ , is related to the engineering constants by the relation

$$K_T = \frac{E_T E_A G_T}{4G_T E_A - E_T E_A - 4E_T G_T v_A^2} \quad (9)$$

where  $E_T$  and  $E_A$  are the transverse and axial Young's moduli of the fiber and  $G_T$  is the transverse shear modulus.

*Interface Model.* Both a linearly elastic and a linearly viscoelastic constitutive relation are considered for the interfacial zone. For the linearly elastic interface, it is assumed that the normal traction between the fiber and matrix phases is proportional to the corresponding normal relative displacement across the interface. Similarly, the tangential traction is taken to be proportional to the tangential relative displacement across the interface. Thus,

$$T_n = k_n [u_n]_I \quad (10)$$

$$T_t = k_t [u_t]_I$$

where

$$\mathbf{u}_n = u_i n_i \mathbf{n} \quad \text{and} \quad \mathbf{T}_n = (\sigma_{ij} n_i n_j) \mathbf{n} \quad (11)$$

$$\mathbf{u}_t = \mathbf{u} - \mathbf{u}_n \quad \text{and} \quad \mathbf{T}_t = \mathbf{T} - \mathbf{T}_n$$

are the normal and tangential displacement and traction vectors respectively,  $[\cdot]_I$  denotes the jump in the relative quantity across the interface,  $k_n$  and  $k_t$  are normal and tangential stiffness parameters arbitrarily taken to be equal in this analysis, and  $\mathbf{T}$  is the traction vector ( $T_i = \sigma_{ij} n_j$ ). Here  $\sigma_{ij} = \sigma_{ji}$  is the Cauchy stress tensor. Since we are considering the plane strain problem, the indices  $i$  and  $j$  in (11) take on the values 1 and 2 referring to the Cartesian coordinate system shown in figure 2. A positive normal relative displacement  $[u_n]_I$  denotes normal separation between the fiber and matrix phases. However, we assume that a negative normal relative displacement  $[u_n]_I$  allows for a physically unrealistic interpenetration of the matrix phase into the fiber phase and, thus, we enforce the impenetrability constraint

$$[\mathbf{u}_n]_I \geq 0. \quad (12)$$

For the linearly viscoelastic interface, the time dependent response of the interfacial zone is taken into account. At each point of the interface, the material response in both the normal and tangential directions is considered to be that of a standard linear solid (SLS). The SLS qualitatively represents the behavior of an idealized cross-linked polymer and can be viewed as a spring in parallel with a spring and a dashpot. The normal and tangential tractions  $T_n$  and  $T_t$  are then related to the relative displacement differences  $[\mathbf{u}_n]_I$  and  $[\mathbf{u}_t]_I$  across the interface by

$$\dot{T}_i + \frac{T_i}{\tau} = (k_i^1 + k_i^2)[\dot{\mathbf{u}}_i] + \frac{k_i^1}{\tau}[\mathbf{u}_i] \quad (13)$$

where the subscript  $i$  is replaced by  $n$  and  $t$  respectively. As for the linearly elastic interface, the normal and tangential stiffness parameters are taken to be equal. Thus,

$$k_n^1 = k_t^1 \text{ and } k_n^2 = k_t^2.$$

For convenience, the time constant,  $\tau$ , in expression (13) is taken to be unity throughout.

### 3. FINITE ELEMENT IMPLEMENTATION

In order to solve the now formulated boundary value problem, the finite element method is employed. Throughout, we assume small displacements. The strain displacement relation then takes the usual form

$$\varepsilon_{ij} = (u_{i,j} + u_{j,i})/2 \quad (14)$$

and the equilibrium equation is written as

$$\sigma_{ij,j} = 0. \quad (15)$$

For the fiber-reinforced composite with an interfacial zone, the Principle of Virtual Work is written as

$$\int_{\Omega} \sigma_{ij} \delta \varepsilon_{ij} d\Omega + \int_S \delta \phi dS = \int_{\Gamma} T_i \delta u_i d\Gamma \quad (16)$$

where  $\Omega$  denotes the interior of the trapezoidal region shown in figure 2,  $I$  is the external traction boundary, and  $S$  is the interfacial traction boundary. The  $\delta u_i$  are the kinematically admissible displacements (satisfying the periodic displacement boundary conditions outlined in section 2 and vanishing on the prescribed displacement boundary). The second term in (16) is the virtual work of separation of the matrix and fiber phases, i.e.

$$\delta\phi = T_n\delta[u_n]_I + T_t\delta[u_t]_I. \quad (17)$$

Note that for the case of a linearly viscoelastic interface, the time dependence of the interface enters into the formulation, and (16) must be discretized in both space and time. A detailed formulation of this discretization is found in Appendix B.

In order to approximately satisfy the impenetrability constraint (12) full Newton Raphson equilibrium iteration is employed with a penalty-like stress update scheme in which the interface is taken to have a suitably high normal stiffness parameter in compression.

#### 4. MACROSCOPIC BEHAVIOR

The numerical results of the present analysis provide a direct method for calculating the effective transverse properties of the fiber-reinforced composite. For the composite with a linearly elastic interface, the numerical results for the effective transverse bulk and shear moduli are compared with the results of Hashin (1989) where the composite cylinder assemblage (CCA) model is employed to obtain the effective transverse bulk modulus, and the generalized self consistent scheme (GSCS) model is used to determine the effective transverse shear modulus. It is noted that the CCA model has been introduced in Hashin and Rosen (1964) and generalized to transversely isotropic fibers and matrix in Hashin (1979). In the context of perfect interface conditions the GSCS model has been applied by Christensen and Lo (1979) to obtain the transverse shear modulus. For the linearly viscoelastic interface, the numerical results are compared with approximate expressions derived analytically for the time dependent transverse properties of the composite.

##### 4.1 *Linearly Elastic Fiber/Matrix Interface*

It can be shown analytically, that due to its inherent elastic symmetry, the hexagonal array composite with linearly elastic constituents is transversely isotropic, see Love (1927), Lekhnitskii (1963). Therefore, we assume that the effective elastic moduli  $C^*_{ijkl}$  are related

to the Cartesian components of the macroscopic or average stress and strain tensors  $\bar{\sigma}_{ij}$  and  $\bar{\epsilon}_{ij}$  in the form

$$\bar{\sigma}_{ij} = C^*_{ijkl} \bar{\epsilon}_{kl}. \quad (18)$$

and that this relation takes the form (7) where the quantities in each expression are replaced by their respective averaged or macroscopic counterparts (eg.,  $\bar{\epsilon}_{11}$  is substituted for  $\epsilon_{11}$ ,  $K_T^*$  for  $K_T$  etc.). We note that when the impenetrability constraint (12) is imposed, the response of the composite is observed to deviate from transverse isotropy when the interface stiffness is low, particularly when it is compared for tensile and compressive loading. For purely tensile loading conditions, this deviation is slight however.

*Numerical Procedure.* Under the condition of CPD loading, the effective transverse shear and bulk moduli of the composite are obtained in the following manner. First, a constant displacement,  $\Delta_2$ , is applied along the external boundary  $EF$  and the displacement,  $-\Delta_2$ , is applied along the external boundary  $AB$  (see fig. 2). The solution of the finite element equations yields the unknown, constant displacement  $\Delta_1$  along the external boundary  $AF$ . The average strain in the  $x_1$  direction is then given by

$$\bar{\epsilon}_{11} = \frac{-4\Delta_1}{3b}. \quad (19)$$

The average strain in the  $x_2$  direction is given by

$$\bar{\epsilon}_{22} = \frac{-4}{\sqrt{3}} \frac{\Delta_2}{b}. \quad (20)$$

By employing the relation (5), the finite element solution also yields the remote applied stress. This is equal to the average stress component  $\bar{\sigma}_{22}$  of the composite. Since there is no applied loading in the  $x_1$  direction, the average stress component  $\bar{\sigma}_{11} = 0$ . Finally, by substituting these averaged quantities into the plane strain constitutive relation (7), the effective transverse shear and bulk moduli are found to be

$$G_T^* = \frac{\bar{\sigma}_{22}}{2 (\bar{\epsilon}_{22} - \bar{\epsilon}_{11})} \quad (21)$$

$$K_T^* = \frac{\bar{\sigma}_{22}}{2(\bar{\epsilon}_{22} + \bar{\epsilon}_{11})}. \quad (22)$$

*Effective Transverse Bulk Modulus.* The numerical results for the effective transverse bulk modulus,  $K_T^*$ , are compared with the results of Hashin (1989) where the CCA model is employed. The CCA expression is given as

$$K_T^* = K_{Tm} + \frac{V_f}{\frac{l}{\bar{K}_{Tf} - K_{Tm}} + \frac{V_m}{K_{Tm} + G_{Tm}}} \quad (23)$$

where  $K_{Tm}$  and  $G_{Tm}$  are the transverse bulk and shear moduli of the matrix, and  $V_m$  and  $V_f$  are the matrix and fiber volume fractions. The quantity,  $\bar{K}_{Tf}$ , is the equivalent transverse bulk modulus of the fiber-interface combination and can be expressed as

$$\bar{K}_{Tf} = \frac{aK_{Tf}k_n}{ak_n + 2K_{Tf}} \quad (24)$$

where  $k_n$  is the normal interfacial stiffness parameter,  $K_{Tf}$  is the transverse bulk modulus of the fiber, and,  $a$ , is the fiber radius. The numerical and CCA results for the effective transverse bulk modulus are shown in figure 3. The effective modulus  $K_T^*$  is plotted versus normalized interfacial stiffness. The normalization is chosen such that

$$k = \frac{k_n}{G_{Tm}a} \quad (25)$$

where  $a$  is the radius of the fiber. As expected, when the impenetrability constraint (12) is not enforced, the numerical and CCA results virtually coincide over the entire spectrum of interface stiffness parameters. However, when this constraint is enforced, the numerical results deviate from the CCA results at relatively low interfacial stiffness parameters. The magnitude of this deviation depends on the loading condition considered in the numerical procedure. It is recalled that in the present analysis  $K_T^*$  is determined by subjecting the hexagonal array model to tensile uniaxial loading. It is noted that when the condition (12) is not imposed, the numerical value obtained for  $K_T^*$  is independent of the loading condition considered.

*Effective Transverse Shear Modulus.* As pointed out by Hashin (1989), the effective transverse shear modulus cannot in general be determined by employing the equivalent fiber-interface concept. Unlike the CCA expression for the effective transverse bulk modulus which is completely independent of the tangential interface stiffness parameter, the effective transverse shear modulus is highly dependent on both stiffness components. However, for the case when both the normal and tangential stiffness parameters are taken to be equal, it is found that the expression for the effective transverse shear modulus obtained by substituting approximate models for the fiber-interface shear modulus into available perfect interface expressions serves as a good approximation over a large range of interfacial stiffness values.

In the present analysis, we employ an approximate expression for the shear modulus of the fiber-interface combination which is written as

$$G_{if} = \frac{aG_{TF}k_t}{ak_t + 2G_{TF}} \quad (26)$$

where  $k_t$  is the tangential interfacial stiffness parameter,  $G_{TF}$  is the transverse shear modulus of the fiber phase, and  $a$ , is the fiber radius. It is noted that when the normal and tangential stiffness parameters are taken to be equal, the result obtained by substituting (26) for the transverse shear modulus of the fiber in the expression of Christensen and Lo (1979) is indistinguishable from the GSCS result of Hashin (1989). In figure 4, the GSCS results obtained by Hashin (1989) are compared with the numerical results. Results obtained by substituting (26) for the shear modulus of the fiber phase in the lower bound expression for arbitrary phase geometry given by Hashin (1979) are also shown in the figure. The effective transverse shear modulus normalized with respect to the shear modulus of the matrix is plotted versus normalized interfacial stiffness. Again, the normalization is chosen as in (25). When the impenetrability constraint (12) is enforced, the numerical results deviate significantly from the GSCS results at relatively low interfacial stiffness parameters. When the constraint (12) is not enforced, the deviation at low stiffnesses is less significant. Again, when (12) is enforced, the magnitude of the deviation depends on the loading condition imposed on the hexagonal array model in the numerical procedure. It is noticed that under these circumstances the modified lower bound expression serves as a good model for the effective transverse shear modulus of the composite. The corresponding results for the effective transverse bulk and shear modulus versus fiber volume fraction for a fixed normalized interfacial stiffness parameter ( $k_t/D$ ) are shown in figure 5.

#### 4.2 Linearly Viscoelastic Fiber-Matrix Interface

In principle, if expressions for the effective moduli of the composite with a linearly elastic interface are known, the correspondence principle can be employed in order to calculate the effective time dependent expressions for the composite with a linearly viscoelastic interface. Unfortunately, the exact elastic expression for the composite under consideration remains to be determined. However, it is noticed that the CCA results for the effective transverse bulk modulus given in the previous section compare closely with the numerical results for a wide range of stiffness parameters over the entire range of volume fractions considered. We thus choose the linearly elastic CCA expression and employ the correspondence principle to obtain a model for the time dependent effective modulus,  $K_T^*(t)$ , of the fiber reinforced composite with a linearly viscoelastic interfacial zone. In order to obtain an analytic expression for the time dependent effective transverse shear modulus,  $G_T^*(t)$ , the modified lower bound expression obtained in the previous section is chosen since it is algebraically simple and lends itself well to analytic Laplace transform inversion. However, it is noted that the usefulness of the resulting time dependent model for the effective transverse shear modulus is limited since it is only good for the special case when the normal and tangential interfacial stiffness parameters are assumed to be synchronous during interfacial stress relaxation.

*Analytical Model.* By substituting the transformed relaxation function of the S.I.S.,  $s\bar{G}(s)$ , into (24) and (26), the transformed expressions  $s\bar{K}_{Tf}(s)$  and  $s\bar{G}_{Tf}(s)$  are obtained. The substitution of these expressions for  $\bar{K}_{Tf}$  and  $\bar{G}_{Tf}$  in the CCA result (23) and the lower bound result of Hashin (1979) yields  $sK_T^*(s)$  and  $sG_T^*(s)$ . Generally a problem arises here in inverting back into the time domain. However, for this relatively simple viscoelastic interface model, the relations for  $K_T^*(s)$  and  $G_T^*(s)$  are easily inverted yielding a model for the time dependent effective moduli  $K_T^*(t)$  and  $G_T^*(t)$ . The effective relaxation function in bulk can be expressed as

$$K_T^*(t) = K_{T\infty}^* + (K_{Tg}^* - K_{T\infty}^*)e^{-t/T_K} \quad (27)$$

while the effective relaxation function in shear can be written as

$$G_T^*(t) = G_{T\infty}^* + (G_{Tg}^* - G_{T\infty}^*)e^{-t/T_G} \quad (28)$$

where  $K_{Tg}^*$  and  $G_{Tg}^*$  are the glassy or instantaneous values for the effective transverse shear and bulk moduli of the composite,  $K_{T\infty}^*$  and  $G_{T\infty}^*$  are the corresponding long term

values obtained as time approaches infinity, and  $T_K$  and  $T_G$  are the respective time constants in transverse bulk and shear. These quantities are defined in Appendix A.

*Comparison of Analytical Model With Numerical Results.* The numerical procedure employed to determine the effective relaxation moduli  $K_T^*(t)$  and  $G_T^*(t)$  is almost identical to that used in the numerical determination of the elastic transverse moduli. The step displacement  $\Delta_2 H(t)$  is applied along the external boundary  $EF$ , and  $-\Delta_2 H(t)$  is applied along the external boundary  $AB$  (see fig.2). Using the relations (21) and (22), the effective moduli are computed and plotted as a function of time. The effective relaxation moduli  $K_T^*(t)$  and  $G_T^*(t)$  predicted by the analytical model and those obtained numerically are plotted for a fixed fiber volume fraction ( $V_f=0.5$ ) as shown in figure 6. The normalized stiffness parameters  $k^1$  and  $k^2$  are varied such that the glassy stiffness of the interface ranges from a normalized value of ( $k_g=10$ ) to a normalized value of ( $k_g=1$ ). Throughout, the ratio of glassy to long-term interfacial stiffness is taken to be ( $k_g/k_\infty=10$ ). The normalization is chosen such that

$$k^i = \frac{k_n^i}{G_{Tm} a} \quad (29)$$

where  $a$  is the fiber radius and the superscript  $i$  takes on the values 1 and 2 referring to the respective chains of the SLS. As shown in the figure, the approximate analytical model compares extremely well with the numerical results over the range where the interfacial stiffness is relatively high. As expected, when the constraint (12) is enforced, for the relatively low glassy stiffness value ( $k_g=1$ ), the numerical results lie below the derived results for the transverse bulk relaxation modulus, and above the derived results for the transverse shear relaxation modulus. It is interesting to note that when the impenetrability constraint (12) is relaxed, the numerical results virtually coincide with the model over the entire range. These results for the Mid-CPD loading direction do not differ significantly.

## 5. MICROSCOPIC BEHAVIOR

In this section, we turn from a macroscopic perspective and focus on the local or microscopic behavior of the transversely loaded fiber-reinforced composite. In particular, we examine the influence of interfacial stress relaxation on the stress fields in the matrix material contiguous to the interface. Throughout, the composite is subjected to a step displacement in the Mid-CPD loading direction, the more severe of the two loading cases

considered, and normalized circumferential stress distributions in the matrix material just outside of the interface are obtained during the numerical simulation of stress relaxation.

During the interfacial stress relaxation, the circumferential stress,  $\sigma_{\theta\theta}$ , normalized with respect to the remote applied stress,  $\sigma_{\infty}$ , is plotted versus angle,  $\theta$ , as shown in figure 7. In the upper diagram, the normalized glassy stiffness of the composite is taken to be ( $k_g=10$ ) and the ration of glassy to long-term stiffness is taken to be ( $k_g/k_{\infty}=10$ ). Again, the time constant,  $\tau$ , is taken to be unity for convenience. As shown in the figure, the normalized circumferential stress increases substantially as time progresses and as the effective stiffness of the interface decreases. Note that as the interface relaxes, a relatively abrupt change in the distributions occurs at approximately 75 degrees. This is due to a local stress concentration at the transitional point where the compressive region of the interface begins. The resulting distributions, as interfacial stress relaxation proceeds, are shown in the lower diagram where the normalized glassy stiffness of the interface is taken to be ( $k_g=1$ ). As time progresses, a noticeable shift occurs in the distributions. The maximum normalized circumferential stress gradually relocates from approximately 75 degrees to approximately the 45 degree mark. In a recent experimental study by Daniel *et al.*, (1989), when a silicon carbide/glass-ceramic composite having closely spaced, near hexagonally packed fibers was transversely loaded, fracture was observed to initiate in the form of radial cracks in the matrix at this 45 degree location.

## 6. CONCLUDING REMARKS

In the present work, the transverse loading of the hexagonal array composite is examined from both a macroscopic and a microscopic point of view. In the macroscopic analysis, the composite is subjected to tensile loading and the effective transverse properties are obtained. For the case of a linearly elastic interface, the numerical results are compared with expressions obtained from the composite cylinder assemblage and generalized self consistent scheme models. It is found that when the impenetrability constraint is imposed, the mechanical behavior of the hexagonal array composite deviates slightly from transverse isotropy and the numerical results deviate significantly from the analytic expressions at low interfacial stiffness values. The magnitude of this deviation depends on the loading configuration considered in the numerical procedure. Note that we impose this constraint to avoid an unrealistic interpenetration of the matrix phase into the fiber phase. For the case of a linearly viscoelastic interface the numerical results for the time dependent transverse moduli are compared with approximate expressions derived analytically. Good agreement

is found among the results over a large range of interfacial stiffnesses. In the micromechanical analysis, normalized circumferential stress distributions are obtained in the matrix material contiguous to the interface during interfacial stress relaxation. It is found that these distributions change substantially as the effective stiffness of the interface decreases. The maximum circumferential stress concentration is found to occur at approximately 45 degrees at relatively low interfacial stiffness values.

*Acknowledgements* – This work was carried out in the course of research sponsored by the U.S. Navy (Contract No. N00014-86-K-0799) under Subcontract No. 89-122 to Northwestern University. Helpful discussions with Professor Z. Hashin, Dr. Han Zhu and Professor I. M. Daniel are gratefully acknowledged.

## REFERENCES

- Aboudi J. (1987). Damage in Composites-- Modeling of Imperfect Bonding. *Composites and Science Technology* **28**, 102–128.
- Achenbach, J. D. and Zhu, H. (1989a). Effect of Interfacial Zone on Mechanical Behavior and Failure of Fiber-Reinforced Composites. *J. Mech. Phys. Solids* **37**, 381–393.
- Achenbach, J. D. and Zhu, H. (1989b). Effect of Interfaces on Micro- and Macro-Mechanical Behavior of Hexagonal Array Fiber Composites. To be published in *J. Appl. Mech.*
- Christensen, R. M., and Lo, K. H. (1979). Solutions for Effective Shear Properties in Three Phase Sphere and Cylinder Models. *J. Mech. Phys. Solids* **27**, 315–330.
- Daniel, I. M., Anastassopoulos, G. and Lee, J. W. (1989). Failure Mechanics in Ceramic Matrix Composites. *Proc. of 1989 SEM Spring Conference on Experimental Mechanics*. Cambridge, MA, 832–838.
- Gosz, M. R. (1989). Effect of a Viscoelastic Interface on the Transverse Behavior of Fiber-Reinforced Composites. M. S. Thesis, Program in Theo. and Appl. Mech., Northwestern University.
- Hashin, Z. (1979). Analysis of Properties of Fiber Composites With Anisotropic Constituents. *J. Appl. Mech.* **46**, 543–550.
- Hashin, Z. (1989). Thermoelastic Properties of Fiber Composites with Imperfect Interface. To be published in *Mechanics of Materials*.
- Hashin, Z. and Rosen B. W. (1964). The Elastic Moduli of Fiber Reinforced Materials. *J. Appl. Mech.* **31E**, 223–232.
- Kriz, R. D. and Stinchcomb, N. W. (1979). Elastic Moduli of Transversely Isotropic Graphite Fibers and Their Composites. *Experimental Mechanics* **19**, 41–49.
- Lekhnitskii, S. G. (1963). *Theory of Elasticity of an Anisotropic Elastic Body*. Holden-Day, Inc., San Francisco.
- Love, A. E. H. (1927). *A Treatise on the Mathematical Theory of Elasticity*. Cambridge.
- Needleman, A. (1987). A Continuum Model for Void Nucleation by Inclusion Debonding. *J. Appl. Mech.* **54**, 525–531.
- Steif, P. and Hoysan, S. F. (1987). An Energy Method For Calculating The Stiffness of Aligned Short-Fiber Composites. *Mechanics of Materials* **6**, 197–210.
- Taylor, R. L., Pister, K. S. and Goudreau, G. L. (1970). Thermomechanical Analysis of Viscoelastic Solids. *Int. J. Numer. Meth. Engng* **2**, 45–59.

## APPENDIX A: DEFINITIONS

In this appendix, we define the quantities contained within the derived expressions (27 and 28) for the time dependent relaxation moduli. The expressions for  $K_{Tg}^*$  and  $G_{Tg}^*$  are obtained by making the following substitutions:

1. Substitute for  $k_n$  in (24) the sum  $(k_n^1 + k_n^2)$  of the stiffness parameters of the SLS obtaining the intermediate expression  $\bar{K}_{Tg}$  for the glassy effective bulk modulus of the fiber-interface combination. Similarly, substitute for  $k_i$  in (26) the sum  $(k_i^1 + k_i^2)$  for the glassy effective shear modulus  $\bar{G}_{Tg}$ .
2. Substitute the expression  $\bar{K}_{Tg}$  into the CCA result (23) and  $\bar{G}_{Tg}$  into the lower bound expression for arbitrary phase geometry of Hashin (1979).

Thus, the effective glassy moduli are written as

$$K_{Tg}^* = K_{Tm} + \frac{V_f}{\frac{I}{\bar{K}_{Tg} - K_{Tm}} + \frac{V_m}{K_{Tm} + G_{Tm}}} \quad (A1)$$

$$G_{Tg}^* = G_{Tm} + \frac{V_f}{\frac{I}{\bar{G}_{Tg} - G_{Tm}} + \frac{(K_{Tm} + 2G_{Tm})V_m}{2G_{Tm}(K_{Tm} + G_{Tm})}} \quad (A2)$$

where

$$\bar{K}_{Tg} = \frac{aK_{Tf}(k_n^1 + k_n^2)}{a(k_n^1 + k_n^2) + 2K_{Tf}} \quad (A3)$$

$$\bar{G}_{Tg} = \frac{aG_{Tf}(k_i^1 + k_i^2)}{a(k_i^1 + k_i^2) + 2G_{Tf}} \quad (A4)$$

and the long-term effective moduli are expressed as

$$K_{T\infty}^* = K_{Tm} + \frac{V_f}{\frac{I}{\bar{K}_{T\infty} - K_{Tm}} + \frac{V_m}{K_{Tm} + G_{Tm}}} \quad (A5)$$

$$G_{T\infty}^* = G_{Tm} + \frac{V_f}{\frac{1}{\bar{G}_{T\infty} - G_{Tm}} + \frac{(K_{Tm} + 2G_{Tm})V_m}{2G_{Tm}(K_{Tm} + G_{Tm})}} \quad (\text{A6})$$

where

$$\bar{K}_{T\infty} = \frac{aK_{Tf}k_n^1}{ak_n^1 + 2K_{Tf}} \quad (\text{A7})$$

$$\bar{G}_{T\infty} = \frac{aG_{Tf}k_i^1}{ak_i^1 + 2G_{Tf}} \quad (\text{A8})$$

Finally, the time constants  $T_K$  and  $T_G$  are written in terms of the time constant,  $\tau$ , of the SLS as

$$T_K = \frac{(k_n^1 + k_n^2)}{k_n^1} \tau \frac{\bar{K}_{T\infty} (1 + m) (\bar{K}_{T\infty} - K_{Tm})}{\bar{K}_{Tg} (1 + m) (\bar{K}_{Tg} - K_{Tm})} \quad (\text{A9})$$

$$T_G = \frac{(k_i^1 + k_i^2)}{k_i^1} \tau \frac{\bar{G}_{T\infty} (1 + n) (\bar{G}_{T\infty} - G_{Tm})}{\bar{G}_{Tg} (1 + n) (\bar{G}_{Tg} - G_{Tm})} \quad (\text{A10})$$

where

$$m = \frac{V_m}{K_{Tm} + G_{Tm}} \quad (\text{A11})$$

$$n = \frac{(K_{Tm} + 2G_{Tm})V_m}{2G_{Tm}(K_{Tm} + G_{Tm})} \quad (\text{A12})$$

## APPENDIX B: FINITE ELEMENT FORMULATION FOR LINEARLY VISCOELASTIC INTERFACE

For the case of a linearly viscoelastic interface, the time dependence of the interface enters into the formulation, and the Principle of Virtual Work

$$\int_{\Omega} \sigma_{ij} \delta \varepsilon_{ij} d\Omega + \int_S \delta \phi dS = \int_{\Gamma} T_i \delta u_i d\Gamma \quad (\text{B1})$$

must be discretized both in space and time. The following implementational details are based on a solution procedure that has been discussed by Taylor, Pister and Goudreau (1970). Writing (B1) in incremental form at time  $t_{n+1}$  yields

$$\int_{\Omega} \Delta \sigma_{ij} \delta \epsilon_{ij} d\Omega + \int_S \Delta T_i \delta [u_i]_I dS = \int_{\Gamma} \Delta T_i \delta u_i d\Gamma - \left[ \int_{\Omega} \sigma_{ij} \delta \epsilon_{ij} d\Omega + \int_S T_i \delta [u_i]_I dS - \int_{\Gamma} T_i \delta u_i d\Gamma \right]_n \quad (B2)$$

where  $(\sigma_{ij})_{n+1} = (\sigma_{ij})_n + (\Delta \sigma_{ij})_n$  and  $(T_i)_{n+1} = (T_i)_n + (\Delta T_i)_n$ . Using (B2) as our starting point, we now express the components  $T_i$  of the interfacial traction vector in terms of the  $[u_i]_I$  as follows. The standard linear solid can be viewed as being comprised of two Maxwell elements in parallel, one of which has an infinite time constant  $\tau$ . The governing differential equation for one Maxwell element is simply expressed as

$$\dot{T}_i^j + \frac{T_i^j}{\tau} = (k_i^j)[\dot{u}_i]_I \quad (B3)$$

where the superscript  $j$  refers to the  $j$ th Maxwell element of the SLS. For extension at a constant rate,  $[\dot{u}_i]_I$ , the exact solution of (B3) is

$$T_i^j(t) = (k_i^j)[\dot{u}_i]_I \tau^j [1 - \exp(-t/\tau)]. \quad (B4)$$

Letting  $(\Delta [u_i]_I)_n = ([u_i]_I)_{n+1} - ([u_i]_I)_n$  and  $\Delta t = t_{n+1} - t_n$ , the interfacial traction components  $T_i$  at time  $t_{n+1}$  are obtained by expressing (B4) in incremental form and summing the partial stresses. Thus

$$(T_i)_{n+1} = \sum_{j=1}^2 \left[ T_i^j \exp(-\Delta t/\tau) + k_i^j \Delta [u_i]_I h(\Delta t) \right]_n \quad (B5)$$

where

$$h(\Delta t) = \tau^j (1 - \exp(-\Delta t/\tau^j)) / \Delta t. \quad (B6)$$

Note that as the time constant,  $\tau^j$ , approaches infinity,  $h(\Delta t)$  in (B6) approaches unity. Referring back to equation (B2), we introduce standard finite element shape functions,  $N$ , and use the arbitrariness of the variations in the nodal displacements to obtain the discrete form

$$\sum_{e=1}^{n_e} \left[ \int_{\Omega} \mathbf{B}_e^T \mathbf{D}_e \mathbf{B}_e d\Omega + \int_S \mathbf{B}_e^T \tilde{\mathbf{D}}_e \mathbf{B}_e dS \right]_{n+1} \Delta \mathbf{d}_e =$$

$$\sum_{e=1}^{n_e} \left[ \int_{\Gamma} \mathbf{N}_e^T \mathbf{T}_{n+1} d\Gamma - \int_S \mathbf{B}^T \mathbf{T}_{n+1} dS - \int_{\Omega} \mathbf{B}^T \boldsymbol{\sigma}_n d\Omega \right] \quad (\text{B7})$$

where, the vector  $\Delta \mathbf{d}_e$  contains the discrete nodal displacement increments and  $n_e$  refers to the number of elements in the model. The first term on the left side of (B7) contains the symmetric gradient operator matrix  $\mathbf{B}_e$  and the plane strain constitutive matrix  $\mathbf{D}_e$ . The second term on the left side of (B7) constitutes the interface stiffness contribution of the interface layer, see Gosz (1989) for interface element formulation. Here, the interface constitutive matrix  $\tilde{\mathbf{D}}_e$  is a 2 x 2 diagonal matrix whose components are given by

$$D_{11} = \sum_{j=1}^2 h(\Delta t) k_n^j \quad (\text{B8})$$

$$D_{22} = \sum_{j=1}^2 h(\Delta t) k_t^j$$

where  $k_n^j$  and  $k_t^j$  are the normal and tangential stiffness parameters associated with the  $j$ th element of the SLS and  $h(\Delta t)$  is defined by (B6). Note that this entire procedure can be easily extended for more general constitutive relations, for example, by modeling the normal and tangential material response of the interface with a greater number of Maxwell elements.

Table 1. Elastic constants of the graphite/epoxy material system considered.

|                | $E_A$ (Gpa) | $\nu_A$ | $E_T$ (Gpa) | $\nu_T$ | $G_A$ (Gpa) | $G_T$ (Gpa) | $K_T$ (Gpa) |
|----------------|-------------|---------|-------------|---------|-------------|-------------|-------------|
| Graphite fiber | 232         | 0.279   | 15.0        | 0.490   | 24.0        | 5.03        | 15.0        |
| Epoxy matrix   | 5.35        | 0.354   | 5.35        | 0.354   | 1.976       | 1.976       | 6.76        |

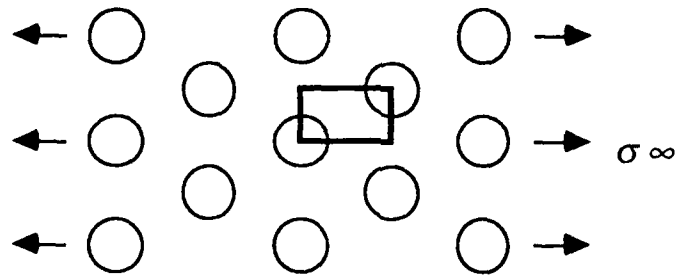


Fig. 1. Mid-CPD loading configuration for the hexagonal array composite.

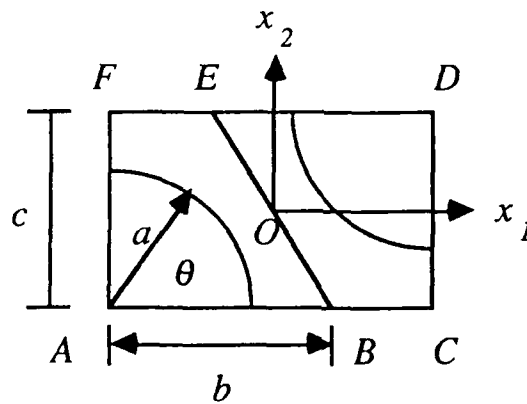


Fig. 2. Schematic of the representative cell of the hexagonal array composite.

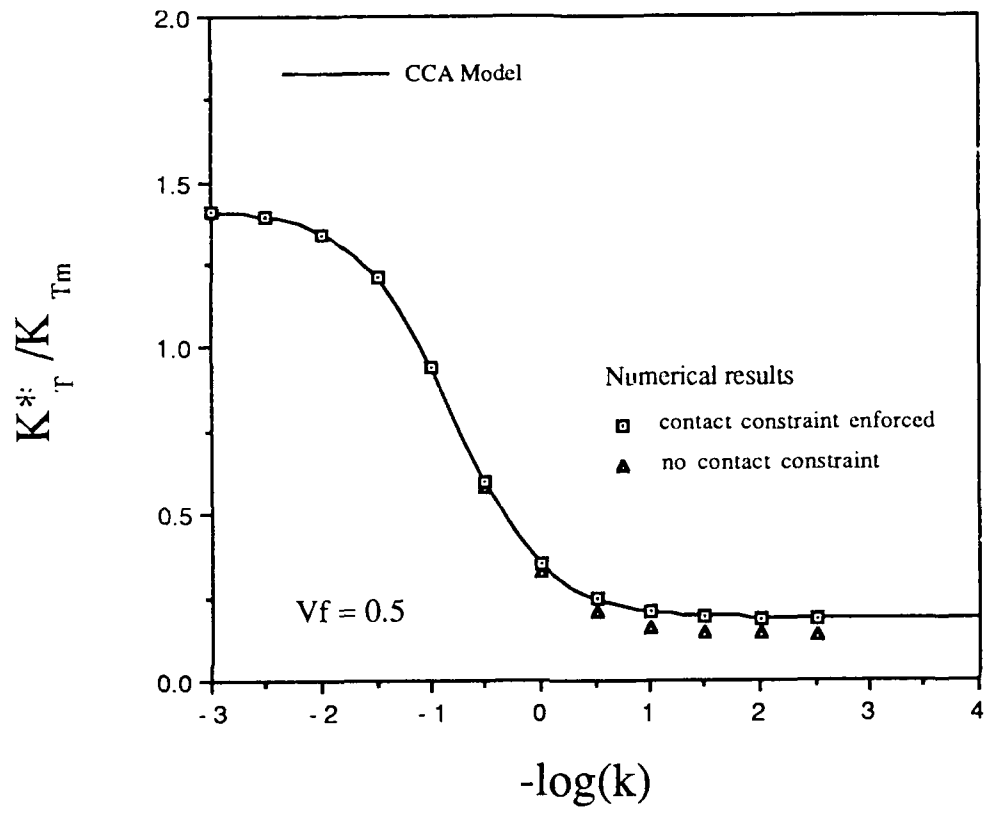


Fig. 3. Normalized effective transverse bulk modulus versus interface stiffness.

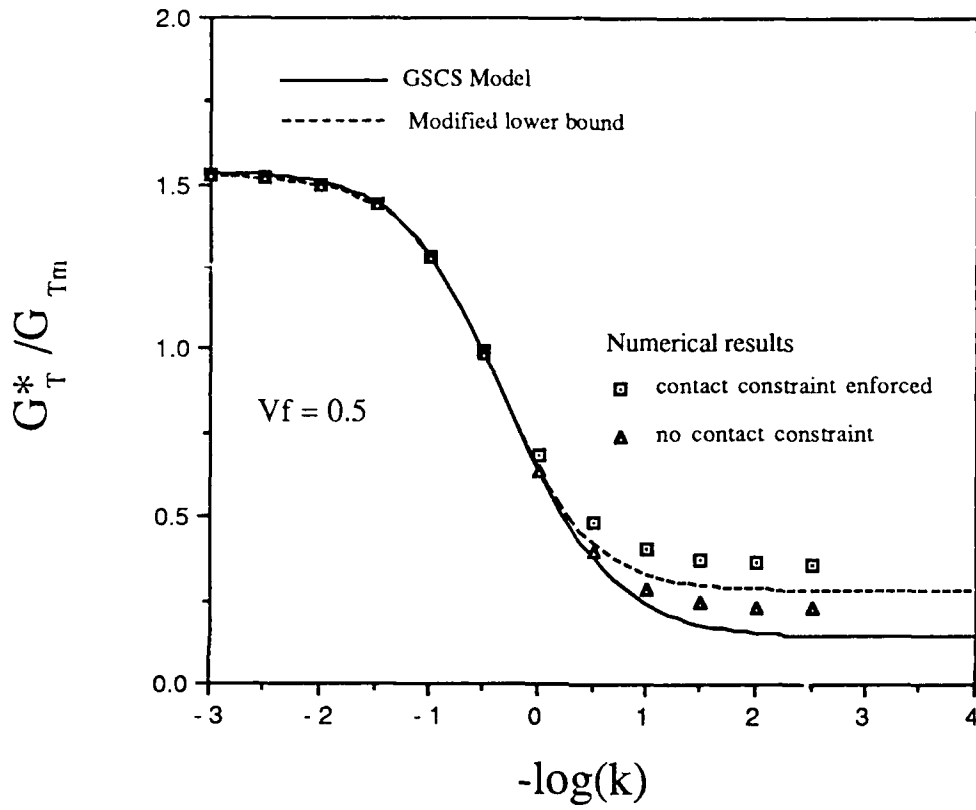


Fig. 4. Normalized effective transverse shear modulus versus interface stiffness.

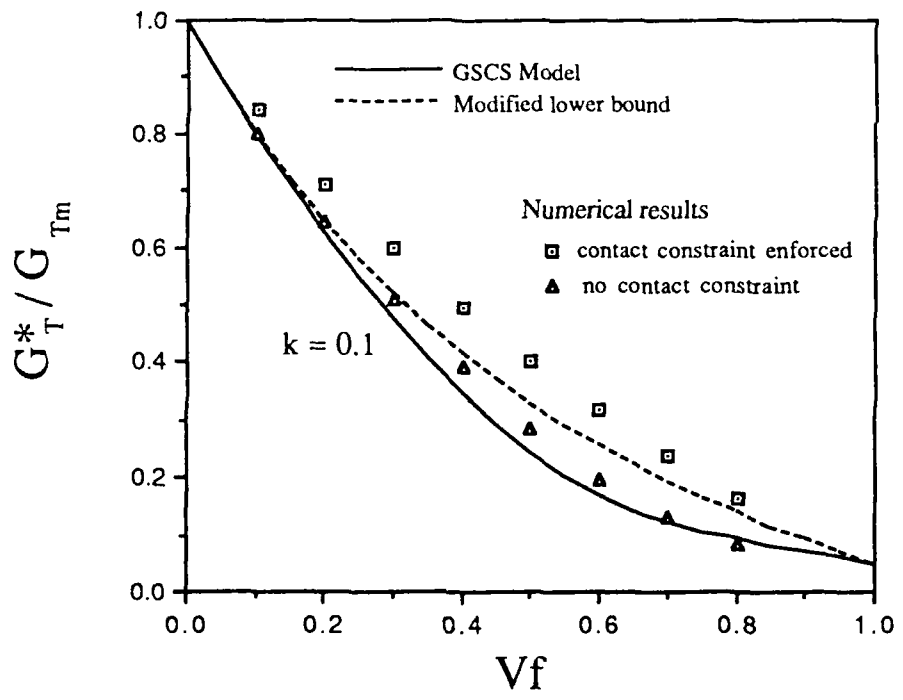
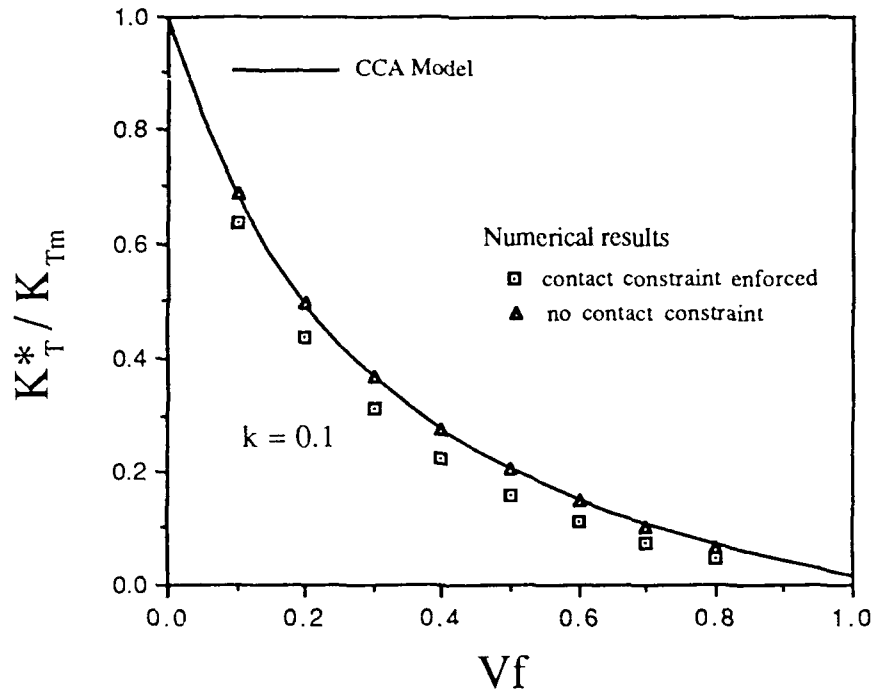


Fig. 5. Normalized transverse bulk and shear moduli versus fiber volume fraction.

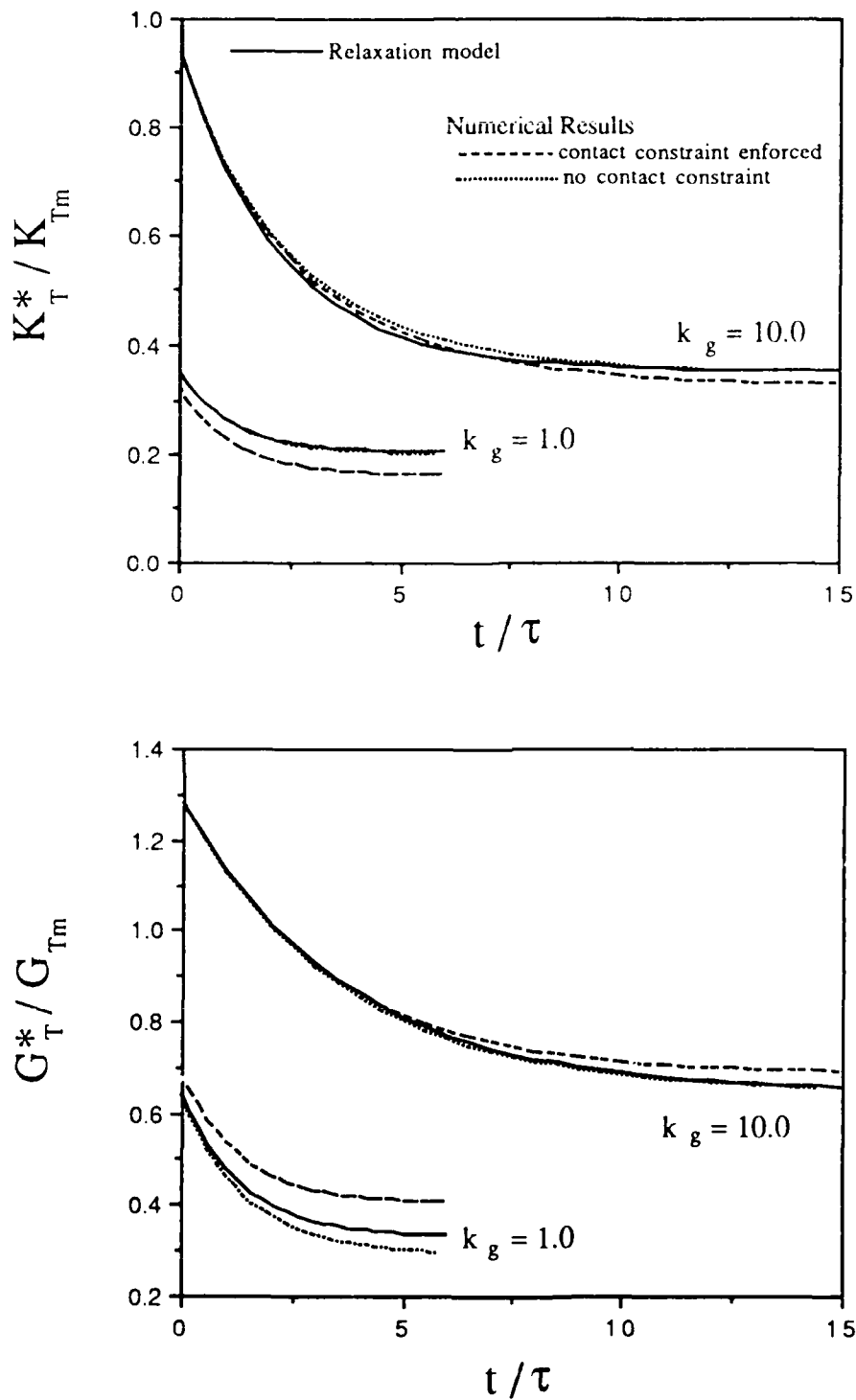


Fig. 6. Comparison of relaxation model in transverse bulk and shear with the numerical results (linearly viscoelastic interfacial zone).

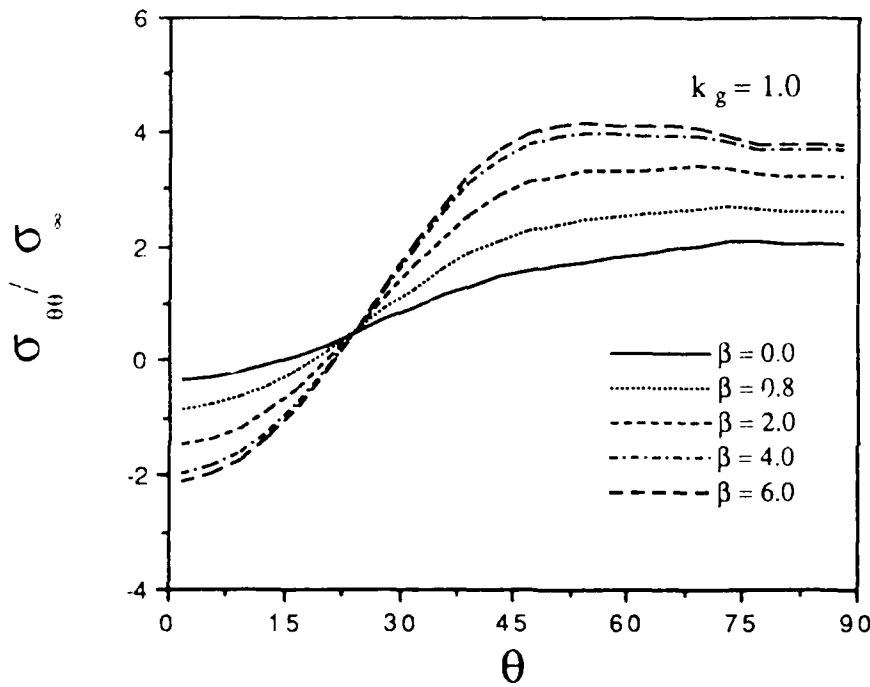
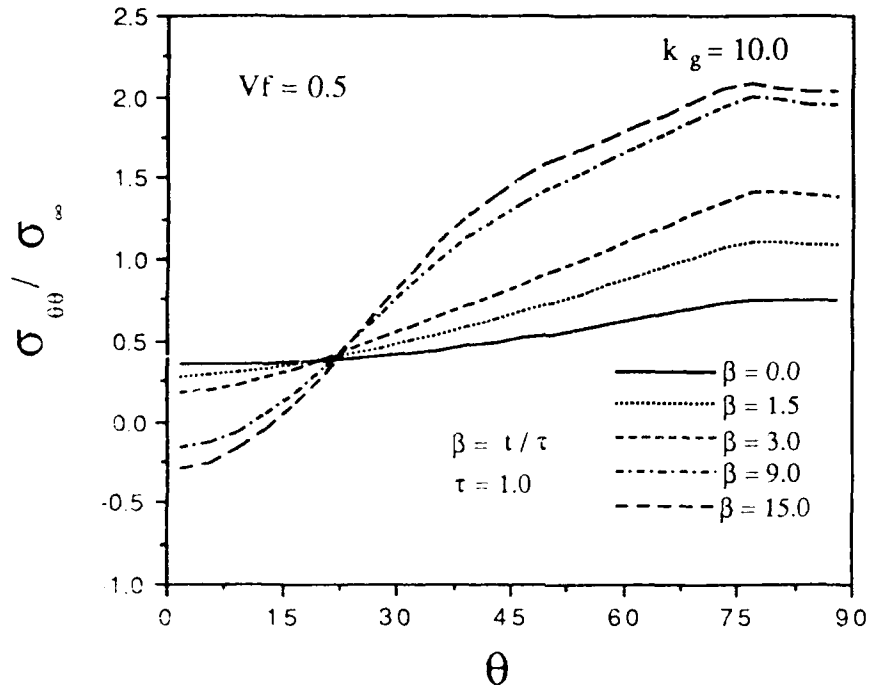


Fig. 7. Normalized hoop stress distributions in the matrix material just outside the interface during stress relaxation.